analytical chemistry

Article

Cite This: *Anal. Chem.* 2018, 90, 2271−2276

pubs.acs.org/ac

MnO_2-Nanosheet-Powered Protective Janus DNA Nanomachines Supporting Robust RNA Imaging

Feng Chen,[§] Min Bai,[§] Yue Zhao, Ke Cao, Xiaowen Cao, and Yongxi Zhao*

Key Laboratory of Biomedical Information Engineering of Ministry of Education, School of Life Science and Technology, Xi'an Jiaotong University, Xi'an 710049, P. R. China

Supporting Information

ABSTRACT: Both biomarker and probe degradations cause serious false assay results. However, protecting a target or a target and a probe simultaneously has rarely been explored. Herein, MnO_2-nanosheet-powered target- and probe-protective Janus DNA nanomachines are reported. It is formed in living cells by an RNA-responsive assembly of two chemically modified DNA partzymes and one substrate probe. MnO_2 nanosheets are used to facilitate the cellular uptake of DNA reagents and generate Mn^{2+}, which are indispensable DNAzyme cofactors for efficient catalytic cleavage. We find that DNA partzymes with modified sugar moieties (e.g., LNA or ones with 2′-O-methylation) protect the RNA of RNA−DNA hybrids from RNase H degradation. LNA blocks RNase H recruitment on the hybrid best because of its 2′-O, 4′-C methylene bridge structure. In contrast, modifications at DNA phosphate moieties fail to protect the RNA. RNA protection can exclude target-degradation-induced false negative results. In addition, the phosphorothioate-modified substrate probe is known to resist nuclease degradation, which minimizes false positive interference. Compared to canonical DNA systems without chemical modifications, the protective Janus nanomachine avoids false results and supports robust RNA imaging.

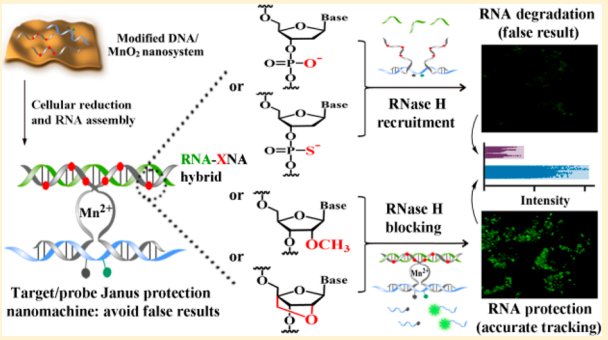

The predictable chemistry and structural programmability of Watson−Crick base pairing makes DNA a widely used material in bioanalysis, nanomedicine, and nanotechnology.[1−3] For DNA-based bioanalysis in living species or complex biological fluids, probe breakdown causes high background noise and false positive results. To circumvent such problems, the well-established method is the use of DNA analogues with chemical modifications, such as phosphorothioate (PS), to oppose nuclease degradation. Nevertheless, target degradation inducing false results is neglected. For instance, cellular RNA levels dynamically change and are determined by the interplay of RNA transcription and degradation.[4] The formation of RNA−DNA hybrids accelerates RNA degradation catalyzed by RNase H.[5,6] As far as we know, neither the protection of only target molecules nor the simultaneous protection of targets and probes from enzyme degradation has been explored.

Recently, we and others have reported that natural 2′-O-methylation (2′OMe) modifications in RNA block its recognition by enzymes including polymerase, ligase, reverse transcriptase, and nuclease.[7−10] Unnatural DNA analogues with unique chemical modifications such as locked nucleic acid (LNA) were also shown to resist nuclease-mediated degradation.[11−13] However, the effects of these modifications of DNA probes to complementary RNA has not been explored. On the other hand, metallic or silicic Janus nanoparticles have been fabricated as molecular motors for catalytic and biomedical applications.[14−17] All these Janus nanoparticles feature two different properties. Inspired by these works, we constructed protective Janus DNA nanomachines to simultaneously prevent target RNA and DNA probes from enzyme degradation for reliable RNA tracking in living cells.

EXPERIMENTAL SECTION

Materials. Tetramethylammonium hydroxide pentahydrate, hydrogen peroxide (H_2O_2, 30 wt %), manganese chloride tetrahydrate ($MnCl_2{\cdot}4H_2O$), and reduced L-glutathione (GSH) were purchased from Sigma-Aldrich (St Louis, MO). All the chemicals were of analytical grade and used as received without further purification. The water and solution used here were RNase-free. The oligonucleotides (Table S1) were synthesized by Sangon Biological Company Ltd. (Shanghai, China), except the substrate probe, which was from TaKaRa Biotechnology Company Ltd. (Dalian, China). The DNA marker, RNase H, and the RNase inhibitor were also obtained from TaKaRa Biotechnology (Dalian, China).

Gel-Electrophoresis Analysis. The protective Janus DNA nanomachine was assembled using miR-21, partzyme A, partzyme B, and D-substrate probe with the molar ratio of 1:5:5:1 μM in 10 μL of RNase H buffer (pH 7.7, 40 mM tris-HCl, 4 mM $MgCl_2$, 1 mM DTT, 4% glycerol, 0.003% bovine serum albumin). The D-substrate probe instead of the substrate

Received: November 9, 2017
Accepted: January 3, 2018
Published: January 3, 2018

DOI: 10.1021/acs.analchem.7b04634
Anal. Chem. 2018, 90, 2271−2276

probe, which has an adenine ribonucleotide (see Table S1), was used here to prevent the destruction of the structure of this nanomachine by DNAzyme cleavage.

Different RNase H treatment conditions, including 1 U of RNase H for 5 min or 0.5 U of RNase H for 20 min at 37 °C, were used to investigate the RNA-protection effect of the partzyme A-OMEs/partzyme B-OMEs probes. To evaluate the RNA-protection effects of different chemically modified partzymes, the condition of 1 U of RNase H for 5 min was selected.

After RNase H cleavage, the reaction products were analyzed by 3.5% agarose gel electrophoresis in 1× TBE buffer at a 70 V constant voltage for 80 min. The gels were visualized by a Syngene G:BOX Imaging System.

Real-Time Fluorescence Monitoring. A LightCycler 96 (Roche Applied Science, Mannheim, Germany) was used to record real-time fluorescence signals and melting curves. The melting temperature (T_m) values of RNA to different chemically modified DNA were analyzed by melting curves. The reactions were performed in 10 μL of annealing buffer (10 mM tris-HCl, 50 mM NaCl, 10 mM $MgCl_2$, pH 7.9) containing 0.5× SYBR Green I and equal concentrations (500 nM) of miR-21, partzyme A, and partzyme B.

To monitor the RNA-protection effects of the partzyme A-OMEs/partzyme B-OMEs probes, 100 nM miR-21, 500 nM partzyme A-OMEs, and 500 nM partzyme B-OMEs were added to 10 μL of RNase H buffer in the presence or absence of 0.1 U of RNase H at 37 °C for 10 min. Partzyme A-DNA and partzyme B-DNA were used as the negative control. Then, the solution was mixed with 10 μL of 2× annealing buffer containing 1000 nM substrate probe to perform DNAzyme cleavage of the substrate probe. Real-time fluorescence signals were recorded at 37 °C for 60 min.

For the performance evaluation of the protective Janus DNA nanomachine, 250 nM partzyme A, 250 nM partzyme B, 500 nM substrate probe, and different concentrations of miR-21 or homologous sequences were involved in typical experiments. The solutions were incubated at 37 °C for 60 min. Similar experiments were performed to analyze miR-155 with its own probes.

Synthesis and Characterization of the MnO_2 Nanosheets. Manganese dioxide nanosheets were synthesized according to previous reports. Briefly, a mixed aqueous solution (20 mL) containing 3 wt % H_2O_2 and 0.6 M tetramethylammonium hydroxide was added to a 0.3 M $MnCl_2$ solution (10 mL) quickly within 15 s under stirring. The dark brown solution was stirred vigorously overnight in the open air at room temperature. Subsequently, the bulk manganese dioxide was collected via centrifugation and then washed with water and methanol. This purification cycle was repeated at least twice. Then, the as-prepared bulk MnO_2 was dried at 60 °C. To produce the MnO_2 nanosheets, 10 mg of bulk MnO_2 was dispersed in 20 mL of water under ultrasonication (>10 h). The shapes and sizes of the MnO_2 nanosheets were examined via an HT7700 transmission electron microscope (TEM, Hitachi, Tokyo, Japan) with a tungsten filament at an accelerating voltage of 100 kV. The size distribution was also characterized by dynamic light scattering (DLS).

Preparation of a MnO_2-Nanosheet−DNA-Probe Composite. The adsorption of the DNA probes on the MnO_2 nanosheets was carried out by mixing the MnO_2 nanosheets with the probes at the desired concentration for 10 min at room temperature. Then, binding buffer (20 mM HEPES, 150 mM NaCl, pH 7.2) was added. The mixture was incubated at room temperature for another 20 min.

Cell Culture. Mammalian cell lines (HeLa, MCF-7, and HEK 293T) were cultured in Dulbecco's Modified Eagle Medium supplemented with 10% heat-inactivated fetal bovine serum and 1% penicillin/streptomycin antibiotics (100 U/mL) in a humidified incubator containing CO_2 (5%) at 37 °C.

Cellular Toxicity Assay of the MnO_2 Nanosheets. The 3-(4,5-dimethylthiazol-2yl)-2,5-diphenyl tetrazolium bromide (MTT) assay was used to evaluate cell viability. MCF-7 cells were seeded in a 96-well microplate with 40 000 cells/well and five wells for each concentration. The cells were incubated at 37 °C for 12 h. Subsequently, the cells were treated with different concentrations of the MnO_2 nanosheets (0−100 μg/mL) at 37 °C for 24 h. The medium was removed, and 10 μL of the sterile-filtered MTT stock solution in PBS (4.0 mg/mL) was added to each well. After 30 min of incubation, absorbance measurements were carried out by using a microplate reader (Tecan Infinite F50).

Microscopic Imaging of Living Cells. Tumor cell lines (HeLa and MCF-7) and a normal cell line (HEK 293T) were seeded in 8-well chambered cover glasses (Cellvis, Mountain View, CA) at 60 000 cells/well at 37 °C overnight and then incubated with 200 μL of serum-free culture media containing 20 μg/mL MnO_2−DNA probe composite (containing 200 nM partzyme A, 200 nM partzyme B, and 400 nM substrate probe) for 6 h. The cells were washed three times with PBS before imaging. All fluorescence images were acquired using Nikon A1 laser-scanning confocal microscopy. A 488 nm laser was used as the excitation source for FAM fluorescence.

Data Extraction by MATLAB. The fluorescence images of the cells were opened by MATLAB, and a series of commands were added in the command-line window to convert the cell images into two-dimensional matrixes that contain the intensity information of three color channels (R: red, G: green, and B: blue). The matrix of the green channel (FAM fluorescence) was used to depict the intensity distribution.

RESULTS AND DISCUSSION

As depicted in Figure 1A, our Janus nanomachine is formed by the RNA-initiated assembly of two chemically modified partzymes and one substrate into an activated DNAzyme. The substrate probe and target RNA are located at opposite sides of our Janus nanomachine. PS modifications in substrate probes are known to resist the nuclease degradation of DNA. Furthermore, we expect chemically modified partzymes are capable of preventing RNase H mediated RNA degradation. Our DNA nanomachine is defined as a Janus system because of these two different nucleic acids' protection properties. The target-stabilized Janus nanomachine can execute recycling cleavage of substrate probes, which enables sustained signal gain. Overall, false results caused by target and probe degradations can be avoided by our Janus nanomachine. The chemical structures of DNA modifications, including PS, 2′OMe, and LNA, are quite different (Figure 1A). Considering low DNAzyme activities in intracellular environments are mainly ascribed to the lack of divalent ion cofactors,[18−20] we use a MnO_2 nanosheet as not only a DNA carrier but also a Mn^{2+} cofactor supplier to enhance the assembly and catalytic performance of the DNA nanomachine.[21,22] Notably, the folded catalytic core sequence of the DNAzyme specifically binds to these cofactors like a pocket for ribonucleotide hydrolysis.

DOI: 10.1021/acs.analchem.7b04634
Anal. Chem. 2018, 90, 2271−2276

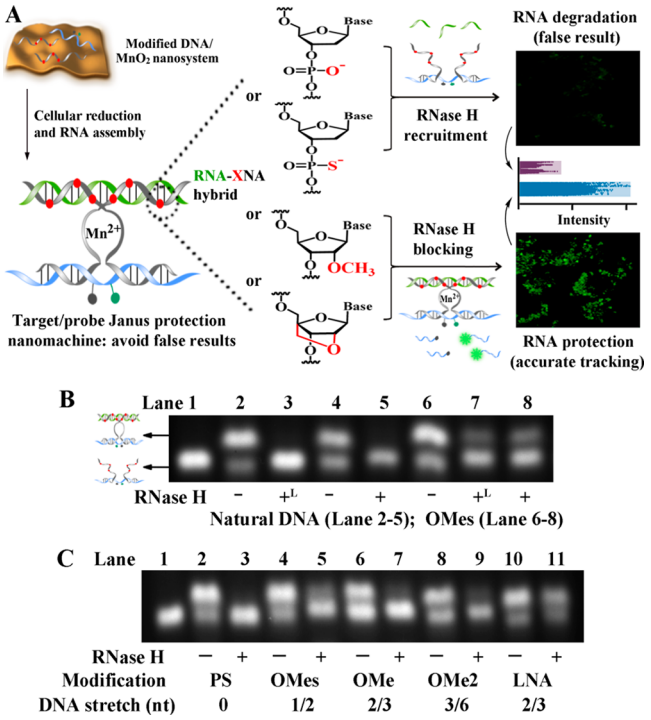

Figure 1. (A) Design and programming of the protective Janus DNA nanomachine. The model cellular-RNA target (green sequence) is miR-21. The chemical structures of a DNA, PS-DNA, 2′OMe-DNA, and LNA monomer are presented, which are highlighted as red circles (red X) in the DNA partzymes (gray sequences). The gray and green circles in the PS-modified substrate probe (blue sequence) are the quencher and fluorophore, respectively. (B,C) Gel-electrophoresis analysis of RNA protection by our Janus nanomachine under different RNase H conditions (B) and chemical modifications (C). The conditions of 1 U of RNase H for 5 min and 0.5 U of RNase H for 20 min at 37 °C are depicted as "+" and "$+^{L}$", respectively.

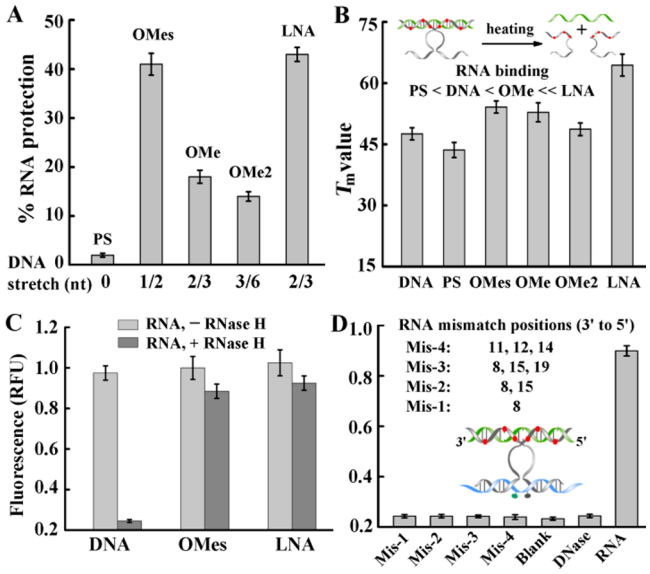

Figure 2. (A) Quantitative evaluation of the gel image in Figure 1C by Quantity One software. (B) T_m values of the hybrids of RNA and different modified probes for the assessment of binding abilities. (C) Fluorescence analysis of the protection-maintained target-RNA catalytic reaction of the Janus nanomachine. (D) Specificity investigation of the Janus nanomachine. The mismatch positions (no hydrogen bonds) of the homologous sequences (green) to the partzymes are numbered from the 5′ ends of homologous sequences. The concentrations of DNase I and the RNA sequences are 5 U/mL and 100 nM, respectively.

First, the protection of target RNA from RNase H mediated degradation was investigated by gel electrophoresis. As shown in Figure 1B, the nanomachine assembled with RNA obtains a bigger molecular weight and size (Lane 2) than it does without RNA (Lane 1), and RNase H mediated cleavage of RNA is observed in RNA-DNA hybrids (Lanes 2−5). In contrast, the 2′OMe/DNA probe protects RNA from degradation in different RNase H conditions (Lanes 6−8, OMes). Comparative analysis using different kinds of chemical modifications (PS, OMes, OMe, OMe2, and LNA) is presented in Figure 1C. Surprisingly, other 2′OMe/DNA probes of decreased 2′OMe numbers together with increased DNA stretches present relatively weak RNA protection (Lanes 6−9, OMe and OMe2). We therefore conclude that long enough DNA stretches in 2′OMe/DNA chimeric probes are required to recruit RNase H. However, this conclusion is not appropriate for PS/DNA probes because nearly all the RNA is cleaved even when a full modified PS probe is used (Lanes 2 and 3). Interestingly, the LNA/DNA probe, containing the same modification number and locations as one 2′OMe/DNA probe (OMe, 2/3 nt), contributes much stronger RNA protection (Lanes 10 and 11). The quantitative evaluation of this gel image is presented in Figure 2A. The 2′OMe/DNA probe with the 1/2 nt DNA stretch presents high RNA protection, whereas the values of the 2/3 and 3/6 nt DNA stretches gradually decrease. Probably, a DNA stretch of >3 nt in a 2′OMe/DNA chimera accelerates the recruitment of RNase H. Nevertheless, a 3 nt DNA stretch in the LNA/DNA chimera can effectively prevent RNase H mediated RNA degradation. These results reveal that LNA inhibits the recruitment of RNase H with higher efficiency than 2′OMe modifications. This is mainly ascribed to the unnatural "locked" structure of a methylene bridge connecting the 2′-O atom and the 4′-C atom, which also causes cytotoxicity. It is worth noting that empirical optimization of modification density, probe concentration, and other conditions may further improve the RNA-protection performance.

It is well-known that introducing chemical modifications changes the hybridization thermodynamics and T_m of oligonucleotides and their complementary RNA or DNA. We therefore determined the T_m values of the natural DNA, PS/DNA, 2′OMe/DNA, and LNA/DNA oligonucleotides with RNA. Compared with the hybrid with the natural DNA, the transition is shifted toward a lower temperature for PS/DNA and higher temperatures for 2′OMe/DNA and LNA/DNA (Figure 2B). The T_m value is raised by <1 °C per 2′OMe modified nucleotide, and a greater increase of ∼2.5 °C per LNA residue is observed. A high T_m value indicates rapid and stable hybridization. Thus, chimeric LNA/DNA and 2′OMe/DNA instead of PS/DNA bind to complementary RNA with higher efficiencies than unmodified DNA, and LNA/DNA presents the highest performance ascribed to locked-ribose-conformation-enhanced base stacking and backbone preorganization. However, LNA modification results in a stronger RNA protection performance, as mentioned above. These data further demonstrate an RNA-protective mechanism based on the blocking of RNase H recruitment, which is determined by the kind and density of chemical modifications. Generally, chemical modifications at sugar moieties (e.g., that in LNA or 2′-O-methylation) instead of phosphate groups contribute

DOI: 10.1021/acs.analchem.7b04634
Anal. Chem. 2018, 90, 2271−2276

good RNA protection. Notably, the effects of modifications at nitrogenous bases are not investigated in this work. Considering the lower cytotoxicity of DNA with natural 2′OMe modifications than that of artificial LNA, we chose the 2′OMe/DNA probe for intracellular analysis.

The RNA-protection-maintaining catalytic reaction of the Janus nanomachine was confirmed by fluorescence analysis (Figure 2C). RNase H degrades the RNA molecules in the RNA−DNA hybrids rather than in the RNA−2′OMe/DNA hybrids. Furthermore, the well-known nuclease resistance of PS-modified oligonucleotide (substrate probe) was also demonstrated, as shown in Figure 2D. Protecting both the target RNA and the DNA probe contributes to improved system stability for reliable analysis, and an excellent sequence specificity for the target RNA (miR-21 here) is achieved by our Janus system (Figure 2D). Single-nucleotide variants are well discriminated, as we reported in previous works, using three-way-junction hybridization structures.[23,24] The binding dynamics of the two partzymes to the substrate probes in the Janus DNA nanomachine were also investigated. Both lengthy and short flanking arms lead to decreased catalytic signals (Figure 3A), which are mainly ascribed to low release rates of the

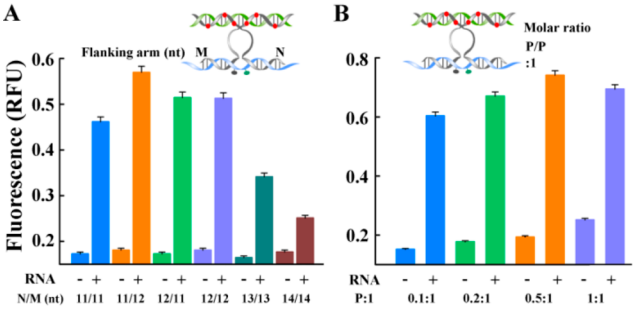

Figure 3. Effect of (A) the binding dynamics of the two partzymes to the substrate probe and (B) the molar ratio of the partzymes to the substrate probe on the catalytic performance of the protective Janus DNA nanomachine.

cleaved probes and poor binding affinities, respectively. A trade-off between binding affinity and release rate is required to obtain high turnover numbers. Additionally, the molar ratio of the partzymes to the substrate probe was evaluated (Figure 3B). Good assay sensitivity toward miR-21 was obtained (Figure S1).

Additionally, we found that intracellular Mg^{2+} levels (~0.5 mM) led to an inconspicuous signal intensity approximately equal to background noise, whereas 0.5 mM Mn^{2+} induced a high catalytic signal (Figures 4A and S2). Therefore, supplying ion cofactors was necessary to enable the catalytic performance of the Janus DNA nanomachine in cellular environments. A MnO_2 nanosheet was used here because of its strong DNA adsorption and the fast generation of Mn^{2+} in living cells.[23,24] Its characterization was shown in Figure 4B by transmission electron microscopy (TEM) and dynamic light scattering (DLS). A lateral-diameter range of 100−200 nm was presented. The reduction of the MnO_2 nanosheet to Mn^{2+} was simulated in vitro by using glutathione (GSH) as a model reductant (Figure 4C). The good biocompatibility of the MnO_2 nanosheet (0−100 μg/mL) was then demonstrated (Figure S3). The highest concentration value allowed the cellular generation of at most 1.2 mM Mn^{2+} to support the

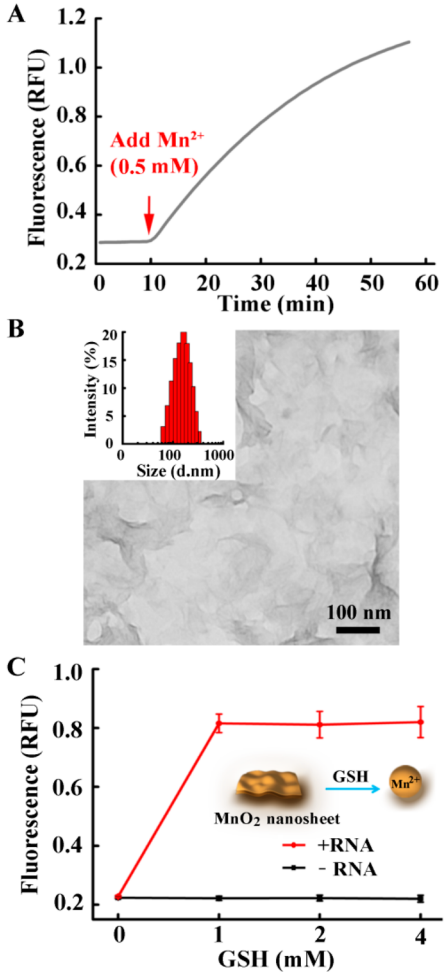

Figure 4. (A) Real-time fluorescence response of the protective Janus DNA nanomachine under the condition of intracellular Mg^{2+} levels (~0.5 mM) and after the subsequent addition of 0.5 mM Mn^{2+}. The curves of Mg^{2+} and Mn^{2+} are merged. (B) Characterization of the MnO_2 nanosheets by TEM and DLS. (C) GSH-induced generation of Mn^{2+} from a MnO_2 nanosheet for catalytic cleavage by the protective Janus DNA nanomachine.

conformational folding and efficient catalysis of the Janus nanomachine.

On the basis of the above results, reliable RNA tracking in living cells was performed with oncogenic miR-21 as a model analyte. Unmodified DNA partzymes are used to assemble target-unprotective nanomachines as a negative control. As depicted in Figure 5A, high fluorescence signals are observed in two tumor cell lines (MCF-7 and HeLa) treated with the Janus nanomachine. In contrast, cells incubated with the target-unprotective nanomachine exhibit much lower fluorescence intensities. These results demonstrate the protection of the target RNA in living cells by the Janus nanomachine. Normal cell line HEK 293T samples treated with both the Janus and target-unprotective nanomachines present dim fluorescence. Furthermore, another negative system, which used control, modified partzymes (noncomplementary with miR-21), also failed to induce visible fluorescence signals (Figure S4). These two results indicate the sequence-specific activation and good RNA protection of the Janus nanomachine in cellular environments. We also used MATLAB software to extract the intensity information for each pixel in the cells of Figure 5A and drew a scatter plot to present the intensity distribution (Figure

DOI: 10.1021/acs.analchem.7b04634
Anal. Chem. 2018, 90, 2271−2276

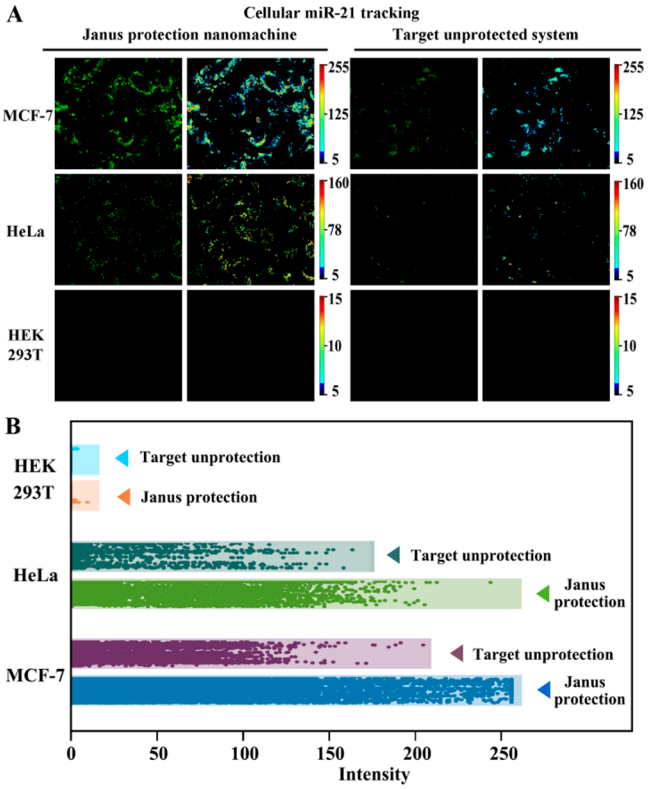

Figure 5. Imaging of miR-21 in living cells. (A) Cell-microscopy images treated with the Janus nanomachine (left panel) and the target-unprotective DNA nanomachine (right panel). The intensity information for each pixel in these images was extracted by MATLAB. (B) Corresponding intensity distribution (vertical direction) of each cell image. High scatter density and intensity values indicate strong fluorescence signals.

5B). These density and intensity data confirmed the good intracellular performance of our Janus nanomachine compared with the target-unprotective nanomachine. As far as we know, the sensitivity and specificity are comparable with those of previously reported works.[20,25−31]

Moreover, the versatility of our Janus protection system was demonstrated by the analysis of other RNA (e.g., miR-155) using two corresponding modified partzymes. As shown in Figures 6 and S5, similar results to those of the miR-21 imaging were obtained. In brief, high fluorescence signals were observed in cancer cells treated with the Janus protection system but not in cells incubated with the target-unprotective system (using unmodified partzymes) as the negative control. It is notable that multiplex RNA analysis in a single cell can be allowed via integrating several sets of probes with MnO_2 nanomaterials to assemble different Janus nanomachines.

Overall, the design, assembly, and activation of the Janus nanomachine as a target- and probe-protection system in living cells are well demonstrated. The nanomachine prevents target-RNA breakdown by RNase H and DNA-probe degradation by deoxyribonucleases, thus avoiding false results. Notably, target-degradation-induced problems have been always neglected, though the protection of probes against nucleases is widely implemented. As far as we know, some previous RNA-imaging methods are based on irreversible DNA assembly or disassembly,[25,27,29,32] and the degradation of target RNA in RNA−DNA hybrids may not disturb reliable assays. However, target-RNA degradation by RNase H could exist in most other

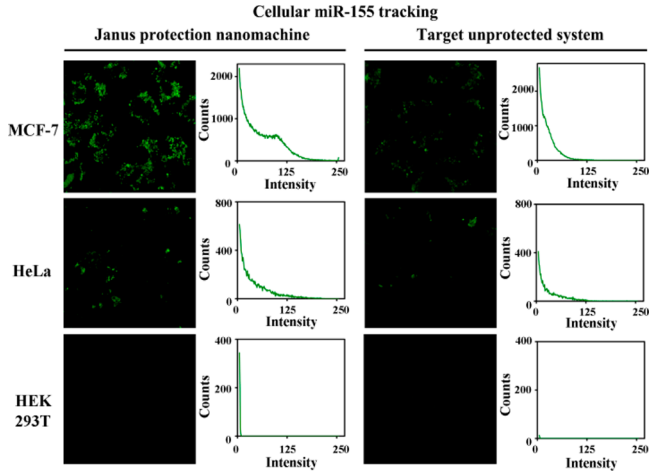

Figure 6. Imaging of miR-155 in living cells treated with the Janus nanomachine or the target-unprotective system. The relationships of the intensity values (>4) and counts (obtained by the Nikon microscopy software) are depicted.

methods, including DNA-hybridization-based[31,33,34] and target-recycled-amplification ones.[20,26,35] This work delineates new possibilities of chemical modifications in biomacromolecules together with integrated nanomaterial−DNA systems[36−41] for biological applications.

CONCLUSION

In conclusion, protective Janus DNA nanomachines were fabricated to prevent target and probe degradations for reliable RNA tracking in living cells. This Janus nanomachine is formed and activated by the RNA-initiated assembly of two chemically modified partzymes and one substrate. Modifications at sugar moieties (e.g., 2′-O-methylation or creation of a 2′-O, 4′-C methylene bridge) instead of at phosphate groups have been demonstrated to block the recruitment of RNase H on RNA−DNA hybrids, thereby preventing RNA degradation. Higher modification densities with lower DNA stretches contributed better RNA protection. Additionally, it is well-known that the PS-modified substrate probe is resistant to nuclease degradation. The simultaneous protection of both the target molecule and the DNA probe minimized assay-system fluctuation and enabled reliable analyses in nuclease-containing, complicated environments. Our work highlights and addresses the neglected issue of target- and probe-degradation-induced false results in living species.

ASSOCIATED CONTENT

Supporting Information

The Supporting Information is available free of charge on the ACS Publications website at DOI: 10.1021/acs.analchem.7b04634.

Oligonucleotides used in this work, real-time fluorescence response of the protective Janus DNA nanomachine under different target-RNA concentrations, M^{2+}-dependent catalysis of the protective Janus DNA nanomachine, cytotoxicity of the MnO_2 nanosheets, negative imaging of miR-21 in living cells, fluorescence information of cells in Figure 6 extracted by MATLAB (PDF)

DOI: 10.1021/acs.analchem.7b04634
Anal. Chem. 2018, 90, 2271−2276

AUTHOR INFORMATION

Corresponding Author

*E-mail: yxzhao@mail.xjtu.edu.cn, Tel.: 86-29-82668908.

ORCID

Yongxi Zhao: 0000-0002-1796-7651

Author Contributions

§F.C. and M.B. contributed equally to this work.

Notes

The authors declare no competing financial interest.

ACKNOWLEDGMENTS

This work was financially supported by the National Science Foundation of China (Nos. 21475102 and 31671013), the China Postdoctoral Science Foundation (No. 2017M613102), the Fundamental Research Funds for the Central Universities (xjj2017039) and the "Young Talent Support Plan" of Xi'an Jiaotong University.

REFERENCES

(1) Chen, Y. J.; Groves, B.; Muscat, R. A.; Seelig, G. *Nat. Nanotechnol.* **2015**, *10*, 748−760.
(2) Surana, S.; Shenoy, A. R.; Krishnan, Y. *Nat. Nanotechnol.* **2015**, *10*, 741−747.
(3) Zhao, Y.; Chen, F.; Li, Q.; Wang, L.; Fan, C. *Chem. Rev.* **2015**, *115*, 12491−12545.
(4) Rabani, M.; Levin, J. Z.; Fan, L.; Adiconis, X.; Raychowdhury, R.; Garber, M.; Gnirke, A.; Nusbaum, C.; Hacohen, N.; Friedman, N.; Amit, I.; Regev, A. *Nat. Biotechnol.* **2011**, *29*, 436−442.
(5) Keskin, H.; Shen, Y.; Huang, F.; Patel, M.; Yang, T.; Ashley, K.; Mazin, A. V.; Storici, F. *Nature* **2014**, *515*, 436−440.
(6) Ohle, C.; Tesorero, R.; Schermann, G.; Dobrev, N.; Sinning, I.; Fischer, T. *Cell* **2016**, *167*, 1001−1013.
(7) Chen, F.; Fan, C.; Zhao, Y. *Anal. Chem.* **2015**, *87*, 8758−8764.
(8) Ji, L.; Chen, X. *Cell Res.* **2012**, *22*, 624−636.
(9) Dong, Z. W.; Shao, P.; Diao, L. T.; Zhou, H.; Yu, C. H.; Qu, L. H. *Nucleic Acids Res.* **2012**, *40*, e157.
(10) Munafo, D. B.; Robb, G. B. *RNA* **2010**, *16*, 2537−2552.
(11) Veedu, R. N.; Vester, B.; Wengel, J. *J. Am. Chem. Soc.* **2008**, *130*, 8124−8127.
(12) Campbell, M. A.; Wengel, J. *Chem. Soc. Rev.* **2011**, *40*, 5680−5689.
(13) Janowski, B. A.; Kaihatsu, K.; Huffman, K. E.; Schwartz, J. C.; Ram, R.; Hardy, D.; Mendelson, C. R.; Corey, D. R. *Nat. Chem. Biol.* **2005**, *1*, 210−215.
(14) Qin, W.; Peng, T.; Gao, Y.; Wang, F.; Hu, X.; Wang, K.; Shi, J.; Li, D.; Ren, J.; Fan, C. *Angew. Chem., Int. Ed.* **2017**, *56*, 515−518.
(15) Gao, W.; Pei, A.; Dong, R.; Wang, J. *J. Am. Chem. Soc.* **2014**, *136*, 2276−2279.
(16) Xuan, M.; Wu, Z.; Shao, J.; Dai, L.; Si, T.; He, Q. *J. Am. Chem. Soc.* **2016**, *138*, 6492−6497.
(17) Li, J.; Hong, C. Y.; Wu, S. X.; Liang, H.; Wang, L. P.; Huang, G.; Chen, X.; Yang, H. H.; Shangguan, D.; Tan, W. *J. Am. Chem. Soc.* **2015**, *137*, 11210−11213.
(18) Cieslak, M.; Szymanski, J.; Adamiak, R. W.; Cierniewski, C. S. *J. Biol. Chem.* **2003**, *278*, 47987−47996.
(19) Zhou, W.; Zhang, Y.; Ding, J.; Liu, J. *ACS Sensors.* **2016**, *1*, 600−606.
(20) Peng, H.; Li, X. F.; Zhang, H.; Le, X. C. *Nat. Commun.* **2017**, *8*, 14378.
(21) Chen, Y.; Ye, D.; Wu, M.; Chen, H.; Zhang, L.; Shi, J.; Wang, L. *Adv. Mater.* **2014**, *26*, 7019−7026.
(22) Deng, R.; Xie, X.; Vendrell, M.; Chang, Y.; Liu, X. *J. Am. Chem. Soc.* **2011**, *133*, 20168−20171.
(23) Zhao, Y.; Qi, L.; Chen, F.; Zhao, Y.; Fan, C. *Biosens. Bioelectron.* **2013**, *41*, 764−770.
(24) Zhang, Q.; Chen, F.; Xu, F.; Zhao, Y.; Fan, C. *Anal. Chem.* **2014**, *86*, 8098−8105.
(25) Li, S.; Xu, L.; Ma, W.; Wu, X.; Sun, M.; Kuang, H.; Wang, L.; Kotov, N. A.; Xu, C. *J. Am. Chem. Soc.* **2016**, *138*, 306−312.
(26) He, X.; Zeng, T.; Li, Z.; Wang, G.; Ma, N. *Angew. Chem., Int. Ed.* **2016**, *55*, 3073−3076.
(27) Cheglakov, Z.; Cronin, T. M.; He, C.; Weizmann, Y. *J. Am. Chem. Soc.* **2015**, *137*, 6116−6119.
(28) Ryoo, S. R.; Lee, J.; Yeo, J.; Na, H. K.; Kim, Y. K.; Jang, H.; Lee, J. H.; Han, S. W.; Lee, Y.; Kim, V. N.; Min, D. H. *ACS Nano* **2013**, *7*, 5882−5891.
(29) Li, L.; Feng, J.; Liu, H.; Li, Q.; Tong, L.; Tang, B. *Chem. Sci.* **2016**, *7*, 1940−1945.
(30) Dong, H.; Ding, L.; Yan, F.; Ji, H.; Ju, H. *Biomaterials* **2011**, *32*, 3875−3882.
(31) Kang, W. J.; Cho, Y. L.; Chae, J. R.; Lee, J. D.; Ali, B. A.; Al-Khedhairy, A. A.; Lee, C. H.; Kim, S. *Biomaterials* **2012**, *33*, 6430−6437.
(32) Wu, Z.; Liu, G.; Yang, X.; Jiang, J. *J. Am. Chem. Soc.* **2015**, *137*, 6829−6836.
(33) Prigodich, A. E.; Randeria, P. S.; Briley, W. E.; Kim, N. J.; Daniel, W. L.; Giljohann, D. A.; Mirkin, C. A. *Anal. Chem.* **2012**, *84*, 2062−2066.
(34) Qiu, L.; Wu, C.; You, M.; Han, D.; Chen, T.; Zhu, G.; Jiang, J.; Yu, R.; Tan, W. *J. Am. Chem. Soc.* **2013**, *135*, 12952−12955.
(35) Wu, C.; Cansiz, S.; Zhang, L.; Teng, I. T.; Qiu, L.; Li, J.; Liu, Y.; Zhou, C.; Hu, R.; Zhang, T.; Cui, C.; Cui, L.; Tan, W. *J. Am. Chem. Soc.* **2015**, *137*, 4900−4903.
(36) Ma, W.; Xu, L.; de Moura, A. F.; Wu, X.; Kuang, H.; Xu, C.; Kotov, N. A. *Chem. Rev.* **2017**, *117*, 8041−8093.
(37) Ma, W.; Sun, M.; Fu, P.; Li, S.; Xu, L.; Kuang, H.; Xu, C. *Adv. Mater.* **2017**, *29*, 1703410.
(38) Ma, W.; Fu, P.; Sun, M.; Xu, L.; Kuang, H.; Xu, C. *J. Am. Chem. Soc.* **2017**, *139*, 11752−11759.
(39) Ma, W.; Kuang, H.; Xu, L.; Ding, L.; Xu, C.; Wang, L.; Kotov, N. A. *Nat. Commun.* **2013**, *4*, 2689.
(40) Fan, H.; Zhao, Z.; Yan, G.; Zhang, X.; Yang, C.; Meng, H.; Chen, Z.; Liu, H.; Tan, W. *Angew. Chem., Int. Ed.* **2015**, *54*, 4801−4805.
(41) Zhao, Z.; Fan, H.; Zhou, G.; Bai, H.; Liang, H.; Wang, R.; Zhang, X.; Tan, W. *J. Am. Chem. Soc.* **2014**, *136*, 11220−11223.

DOI: 10.1021/acs.analchem.7b04634
Anal. Chem. 2018, 90, 2271−2276